JOURNAL OF APPLIED ELECTROCHEMISTRY 10 (1980) 365–377

The anodic formation and cathodic reduction of cuprous oxide films on copper in sodium hydroxide solutions

S. L. MARCHIANO, C. I. ELSNER, A. J. ARVIA

Instituto de Investigaciones Fisicoquímicas Teóricas y Aplicadas, División Electroquímica, Sucursal 4 – Casilla de Correo 16, 1900 La Plata, Argentina

Received 15 June 1979

The potentiodynamic response of the Cu/alkaline solution interface in the potential range where Cu_2O is formed and reduced has been investigated using a broad range of experimental conditions, including different electrode treatments. The reproducibility of the results is also critically considered. The cathodic reaction revealed that at least three different Cu(I) species are formed during the Cu_2O formation. One of them has been attributed to a soluble Cu(I) species. One out of the two remaining Cu(I) surface species undergoes potentiostatic ageing effects. The results are discussed in terms of previously proposed reaction mechanisms related to the Cu_2O formation and reduction.

1. Introduction

The number of publications on the electrochemical behaviour of copper in alkaline aqueous solutions is relatively large [1–14]. A review of the literature up to about 1972 can be found in [1]. It shows that the emphasis of the electrochemical studies was on the electroformation of Cu(II) despite the interest in Cu_2O formation as the probable first product in the anodic oxidation of copper.

The electrochemistry of the copper/alkaline solution interfaces involves different solid phases comprising the formation of Cu(I), Cu(II) and Cu(III) species, within definite potential ranges between the hydrogen evolution potential and the oxygen evolution potential. The complexity of the processes applies even within the more restricted potential range corresponding to the anodic formation and cathodic reduction of the cuprous oxide species. The formation of Cu_2O within a definite potential range in alkaline solutions has been demonstrated by electron diffraction [3], X-ray diffractometry, scanning electron microscopy [10], electroreflectance spectroscopy [12], transmission electron micrograph [11] and ellipsometry [9, 13]. In principle, despite the agreement of the numerous results reported during the past years concerning the identification of the main solid species produced during the anodic reaction, the interpretations advanced for the mechanism of the various reactions vary considerably particularly when one attempts to derive the finer details of the electrochemical response of copper in alkaline solutions. Thus, from the kinetic viewpoint the electrochemical reactions involving either the formation or the reduction of Cu_2O require further investigation to elucidate the type of reactions related to Cu(I) and Cu(II) formation, whether they are formed by consecutive or concurrent reactions, to detect the possible formation of an appreciable amount of soluble Cu(I) species during the electrochemical formation of Cu_2O, to determine the formation of OH^--containing species as precursors to the Cu_2O formation and to demonstrate the contribution of ageing processes during the electrode reaction. This is, to some extent, related to the fact that the reproducibility of a polycrystalline copper surface in electrochemical measurements depends markedly on the electrode pre-treatment. The corrosion stability of electropolished surfaces as compared to mechanically polished ones can be shown to depend on the different structure and properties of the oxide film formed on the electrode by the various treatments and to differences in microgeometries. This includes different degrees of surface smoothing, elimination or preservation of the surface layer

0021–891X/80/030365–13$03.30/0

deformed during the mechanical treatment and the formation of passive films differing in structure and chemical composition [16–19].

The present work attempts to elucidate some of the ambiguities reported on the electrochemical behaviour of the Cu/alkaline solution interface and to distinguish the degree of participation of mechanisms such as the dissolution–precipitation mechanism [7, 9, 11, 13] and the solid state nucleation and growth mechanism [6, 12] in the electrochemical reaction.

2. Experimental

A conventional Pyrex glass electrolysis cell was employed. The working electrode was a polycrystalline copper disc (Cu 99.9% purity) built by placing a copper rod (1 mm diameter) axially within a Teflon rod (1.8 cm diameter). The flat disc (active and inactive portions) was finished on a precision lathe. Occasionally copper wire electrodes (0.5 and 0.9 mm diameter) were also employed. The counter electrode was a large platinum sheet and a SCE electrode was used as a reference electrode. The following working electrode pre-treatments were used before immersion in the alkaline electrolyte. (a) The electrode was firstly degreased, rinsed with water, then mechanically polished with a fine alumina powder suspension in a water–ethanol mixture and finally rinsed several times with triply distilled water. (b) The electrode was only etched in a (1 : 1) aqueous H_2SO_4 solution for 30 min. (c) The same as (b) but using an aqueous HNO_3 solution (1 : 1) for 15 min. (d) The electrode was firstly thermally oxidized in air and then left in contact with the electrolyte solution.

The following electrolyte solutions were employed: x M NaOH (10^{-2} M $\leqslant x \leqslant$ 1 M) and x M NaOH + y M $NaClO_4$ (10^{-2} M $\leqslant x \leqslant 10^{-1}$ M and 10^{-1} M $\leqslant y \leqslant$ 1 M). The solutions were prepared by dissolving the anhydrous chemicals (AnalaR quality) in triply distilled water. Oxygen was purged from the cell solution using bottled nitrogen of the highest commercial purity. Traces of oxygen were removed from the gas by flowing through a heated tube containing finely divided metallic copper. Before entering the cell the gas was passed through two washing towers one containing AnalaR quality 98% H_2SO_4 (Mallinckrodt) and another containing the same electrolyte as in the cell.

The experiments were carried out in the 25° C to 60° C range. The electrochemical interface was perturbed with either simple or complex potential–time programmes. The potential sweep rate of the linear potentiodynamic experiments covered from 0.05 V s^{-1} up to 10 V s^{-1}. The scheme of the complex potential perturbation functions is included in each potentiodynamic E/I display.

3. Results

The nth sweep cyclic voltammogram run between −1.3 V and 0 V at 0.1 V s^{-1} (Fig. 1) shows during the positive-going potential sweep a first anodic current peak (API) followed by a complex current peak (APII). At higher positive potentials (not shown in Fig. 1), in the potential range where the oxygen evolution starts, the conjugate current peaks related to the soluble redox Cu(II)/Cu(III) couple can be distinguished [7, 8, 14]. The negative-going potential scan presents two cathodic current peaks (CPI and CPII), and at potentials more negative than those of CPI an apparently cathodic limiting current is observed in the −0.9 V to −1.2 V range. The characteristics of the above described current peaks depend on many variables such as the type of electrode pre-treatment, the number of initial potential cycles, the alkali concentration, the total ionic strength, the switching potentials, ($E_{\lambda,a}$ and $E_{\lambda,c}$), the rate of the potential perturbation and the stirring conditions.

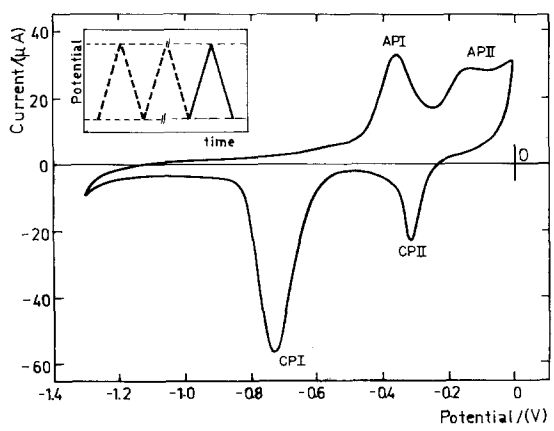

Fig. 1. Stabilized potentiodynamic E/I profiles at 0.1 V s^{-1}. 0.1 M NaOH, 25° C. Electrode area 0.0314 cm^2.

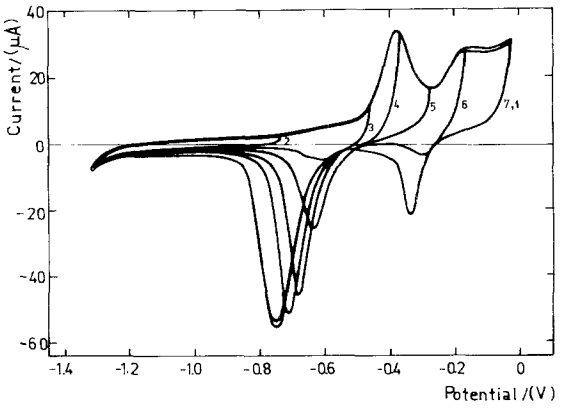

Fig. 2. Influence of $E_{\lambda,a}$ on the stabilized E/I profiles at 0.1 V s^{-1}. 0.1 M NaOH, 25° C. The numbers indicate the sequence of the runs. Electrode area 0.0314 cm^2.

A gradual change of the potentiodynamic E/I displays is noticed during the first potential scans but a stable E/I profile is attained after 30 min potential cycling at 0.1 V s^{-1} within the potential range of Cu_2O formation and reduction. Thus, during the first positive-going potential excursion the height of API may be larger than that of APII. However, during continuous potential cycling, the height of the former peak gradually decreases while that of the latter increases to attain a stable profile. The initial rate of change of both current peaks upon cycling depends on the potential range covered during the potentiodynamic perturbation.

The negative-going potential excursion shows that the height and potential of CPI depends on $E_{\lambda,a}$ (Fig. 2). As the latter becomes more positive up to about −0.17 V the height of CPI increases but its potential becomes more negative. However, a stable CPI display is observed when $E_{\lambda,a}$ extends beyond about −0.2 V. It is interesting to observe that CPII begins to appear only when the current associated with APII is recorded. Similarly to CPI, the potential corresponding to CPII becomes more negative as $E_{\lambda,a}$ is fixed at more positive potentials. The following E/I displays are confined to the potential range of the Cu/Cu_2O system. The main current peaks, namely API and CPI, are covered when the potentiodynamic experiments are performed in the −1.3 V to −0.30 V range.

The influence of the electrode pre-treatment plays an outstanding role in the reproducibility of the experimental results in the Cu/Cu_2O potential range. The E/I characteristics of differently pre-treated copper electrodes in 1 M NaOH, which are perturbed with symmetric triangular potential sweeps, are compared in Fig. 3. Thus, with a mechanically polished electrode both the positive- and negative-going potential sweeps exhibit a more complex E/I display (Fig. 3a). Furthermore, the anodic current peak related to the Cu_2O formation is broad and flat. In contrast, the reduction current peak is well defined and relatively symmetric. Repetitive potential cycling during a relatively long period makes the E/I profile become somewhat simpler (Fig. 3b). On the other hand, when HNO_3 etched electrodes are used (Fig. 3c) the contribution of the minor processes diminishes appreciably during the first potential sweep and practically disappears after repetitive potential cycling (Fig. 3d). When this occurs the anodic current peak is well defined and symmetric whilst the reduction current peak is broad and it becomes appreciably asymmetric. The electrode pre-treated with H_2SO_4 exhibits clean and well-defined anodic E/I displays and broad cathodic current peaks involving contributions from at least two reduction processes that are only distinguished when the potential sweep rate of the negative-going potential excursion decreases (Fig. 4). Moreover, the negative-going potential excursion shows initially an anodic current peak which is in exactly the same potential range as current peak API. The E/I display run with electrodes etched in diluted HNO_3 and with a symmetric triangular potential sweep are similar to those reported with the H_2SO_4 etching. The magnitude of both the anodic and the cathodic charge decreases as v increases. The limiting value extrapolated at $v \to \infty$ is about 2 mC cm^{-2}. Under these circumstances the anodic-to-cathodic charge ratio (Q_a/Q_c) is 1.00 ± 0.25 at any potential sweep rate between 0.05 V s^{-1} and 0.5 V s^{-1}.

The heights of API and CPI increase with the potential sweep rate for the different NaOH concentrations and the log (current peak height) versus log v plot (Fig. 5) indicates that the heights of both current peaks are proportional to v^x where x is equal to 0.7 for CPI peak and to 0.66 for API. Either the height of API divided by Q_a, the total anodic charge, or the height of CPI divided by Q_c, the total cathodic charge, fit a first order dependence on v. The potential of API determined from the first potential sweep shifts towards more positive values as v increases and simultaneously, the

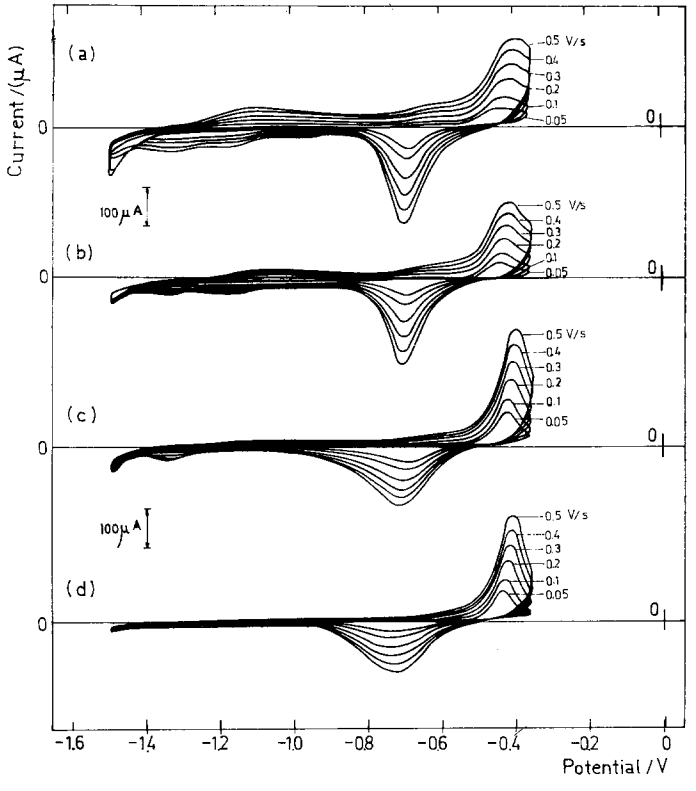

Fig. 3. Influence of the copper electrode pre-treatment on the potentiodynamic *E/I* displays. 1 M NaOH, 25° C. Electrode area 0.0314 cm^2. (a) alumina polishing; (b) as in (a) plus a 20 min potential cycling at 0.2 V s^{-1}; (c) alumina polishing and etching in a 1 : 1 HNO_3 solution; (d) as in (c) plus a 20 min potential cycling at 0.2 V s^{-1} before recording the *E/I* display.

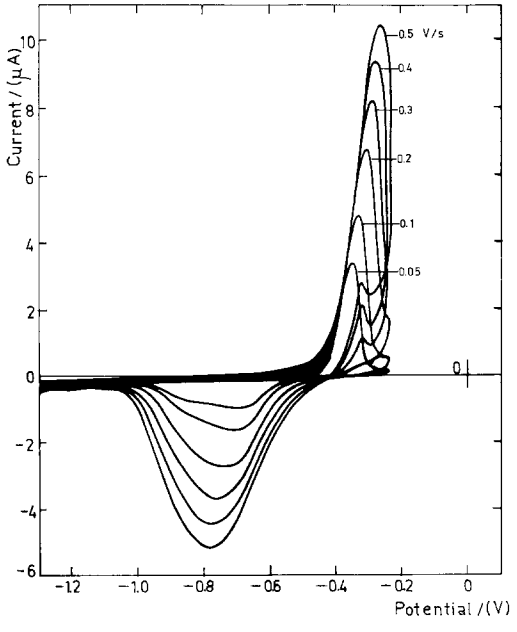

Fig. 4. Stabilized potentiodynamic *E/I* profiles run at different potential sweep rates ($v_a = v_c$). The copper electrode was previously etched in a 1 : 1 H_2SO_4 solution. 0.1 M NaOH, 25° C. Electrode area 1.39 cm^2.

potential of CPI becomes more negative as v increases. Both peak potentials change linearly with the logarithm of v (Fig. 6). The corresponding slopes are relatively low and depend on the electrode pretreatment and perturbation conditions, as shown in the figure. In general, the lowest slopes

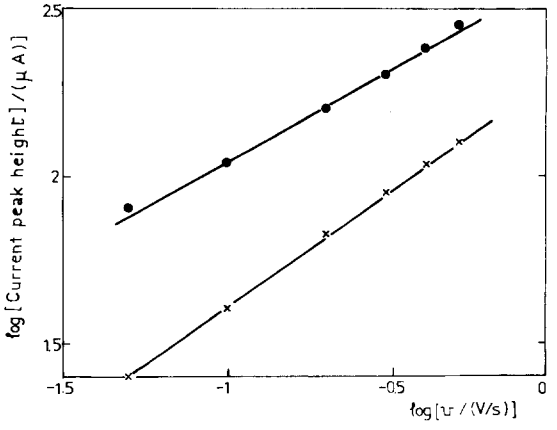

Fig. 5. Log (height API) versus log v relationship. 1 M NaOH, 25° C. × Electrode pre-treatment (c) and • (d) as described in Fig. 3. Electrode area 0.0314 cm^2.

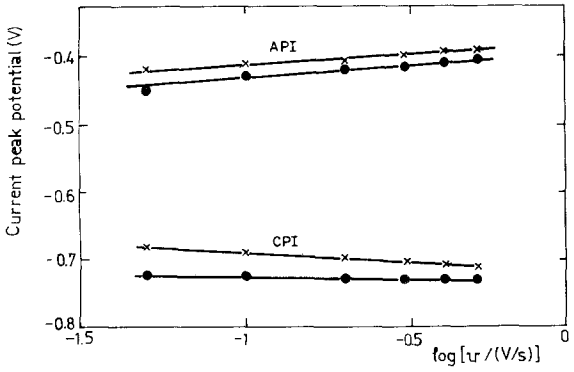

Fig. 6. Log (current peak potential) versus log v relationship. 1 M NaOH, 25° C. × Electrode pretreatment (c) and • (d) as described in Fig. 3.

are obtained when the electrochemical interface is potential cycled for a prolonged period. Moreover, the intersection of the straight lines corresponding to the conjugate processes coincides well with the thermodynamic potential of the Cu/Cu_2O redox couple which at pH 14 is -0.59 V. During cycling the potential of CPI remains constant.

The triangular potential sweep E/I displays run with a constant v_a and different v_c show that the potential of CPI shifts towards more negative potentials as v_c increases (Fig. 7). At a constant v_c, the height of CPI increases as v_a decreases.

The heights of API increases with the NaOH concentration in the solutions containing only one electrolyte (Fig. 8). But in those solutions where $NaClO_4$ was added, it appears that these peak heights are practically independent of the NaOH concentration.

The shape of the E/I profiles depends on the total ionic strength (Fig. 9), where the arrows indicate the gradual changes of the repetitive E/I profile run at 0.1 V s^{-1} from $E_{\lambda,c} = -1.30$ V to an $E_{\lambda,a}$ value where the Cu(II) species start to be formed. When the behaviour of the NaOH solutions is compared to that of the solutions containing $NaClO_4$, these changes of the E/I profiles are opposite although in both cases they depend on v as well as on the switching potential values. The larger the ionic concentration apparently the simpler, non-structured and more symmetric the cathodic E/I profiles that result. The multiplicity

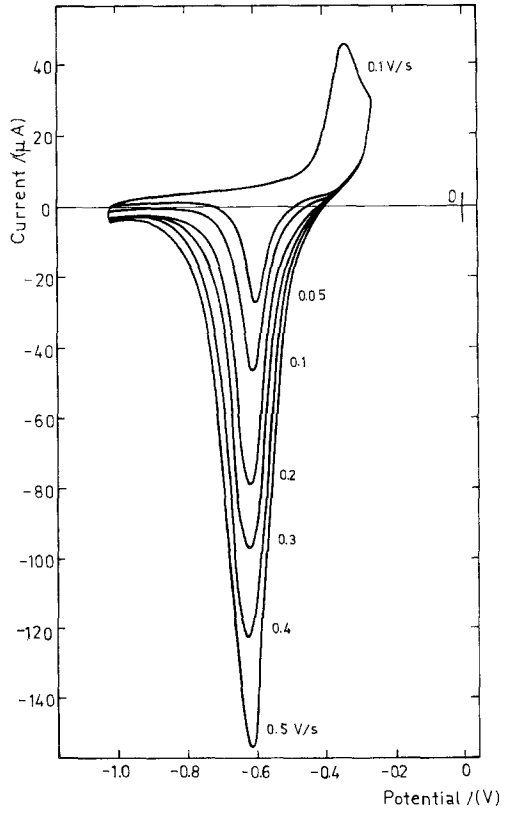

Fig. 7. Stabilized potentiodynamic E/I profiles run at a constant v_a and different v_c. 0.1 M NaOH + 0.5 M $NaClO_4$, 25° C. Electrode area 0.0314 cm^2.

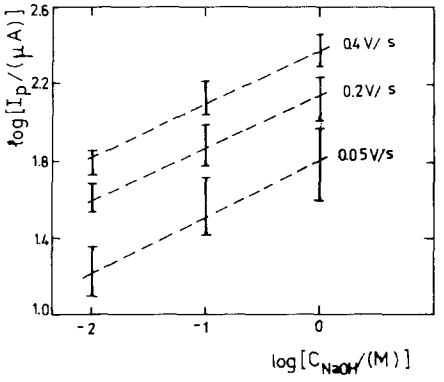

Fig. 8. Log (API height) versus log (NaOH concentration) plot for electrolytes without supporting electrolyte. 25° C, electrode area 0.0314 cm^2.

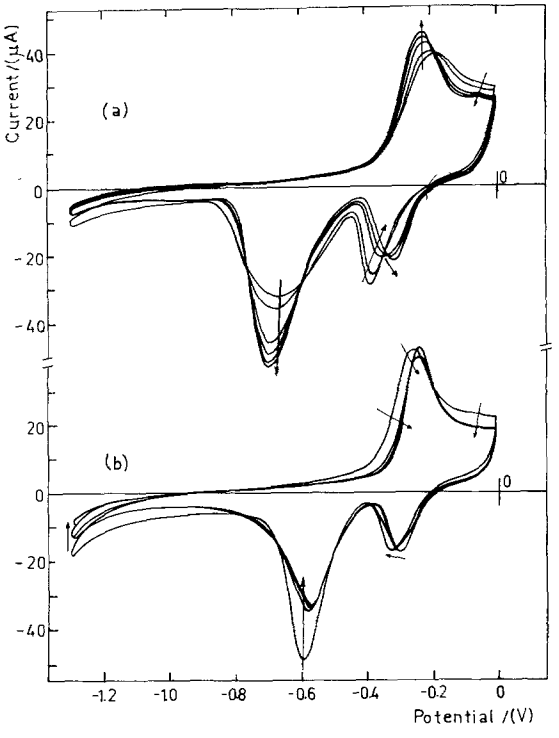

Fig. 9. Repetitive triangular potential sweep E/I profiles at 0.1 V s^{-1}. (a) 0.01 M NaOH; (b) 0.01 M NaOH + 1 M $NaClO_4$, 25° C. The E/I displays were recorded at 5 min intervals and the arrows indicate the direction of the changes produced in the E/I profiles during cycling. Electrode area 0.0314 cm^2.

of the cathodic current peaks in the potential range of the reduction of the Cu(I) species can also be related to the characteristics of the E/I displays obtained either at a constant v_a and different v_c or at different v, but $v_a = v_c$ (Figs. 4 and 7). For the latter at constant E_λs the shift of the anodic process towards more positive potentials as v increases implies that smaller Q_a and Q_c values are involved as v_a increases. The complexity of the cathodic current peak becomes clearer as Q_a decreases and v_c increases. These effects should be related to changes of either the composition or the structure of the film or of both simultaneously.

The E/I contours are also strongly sensitive to the temperature (Fig. 10). As it increases the charges corresponding to API and CPI increase, the current peaks become thinner and increase in height, but almost no difference between the peak potentials is observed (Figs. 10a and b). Another important feature of the E/I displays appears when the same electrode is firstly potential swept at 25° C, then at 45° C and finally again at 25° C, without it having been removed from the cell solution (Fig. 10). The thermal cycle produced a noticeable change in the E/I contour. Thus, the reduction contour involves at least two additional cathodic current contributions on both sides of the main reduction current peak CPI. This further proves that the electrochemical reaction is very sensitive to changes on the metal side of the electrochemical interface.

Moreover, runs made at a constant v from a fixed cathodic switching potential, using repetitive triangular potential sweeps with progressively increasing anodic switching potentials (Fig. 11), yield information about the genesis of the multiplicity of the anodic and cathodic current peaks. As $E_{\lambda,a} = -0.44$ V the reduction current peak is broader than the one found for $E_{\lambda,a}$ more positive than -0.44 V. As $E_{\lambda,a}$ further increases to cover the potential range of API, the current peak CPI increases in height and shifts towards more negative potentials. In relation to these results the current contribution at the positive potential side of the CPI is more evident when $E_{\lambda,a}$ is located in the potential range preceding that of API and v exceeds 1 V s^{-1} (Fig. 12). It is also interesting to observe that depending both on $E_{\lambda,a}$ and v, the negative-going potential excursion from $E_{\lambda,a}$ exhibits an anodic current contribution as a small current peak which coincides with the API. At a constant $E_{\lambda,a}$ higher v enhances this current contribution. This effect is associated with the incomplete Cu(I) layer formation, due to the initiation of the anodic process which occurs at more positive potentials as v_a increases.

The complex dependence of the CPI potential on $E_{\lambda,a}$ is similar to that found for other film-forming electrochemical systems involving ageing. Therefore, the appearance of the electroreduction current peak as $E_{\lambda,a}$ increases, shows that the anodic oxidation of Cu to Cu(I) ascribed to the potential range of current peak API probably involves several species of different reactivity.

To determine further details of the reduction of the possible different species anodically produced, various complex potential–time perturbations were applied to the electrochemical interface. One of them consists of a triangular potential excursion starting at $E_{\lambda,c}$ after holding the potential at E_τ (-0.525 V $\leqslant E_\tau \leqslant -0.440$ V) during a lapse

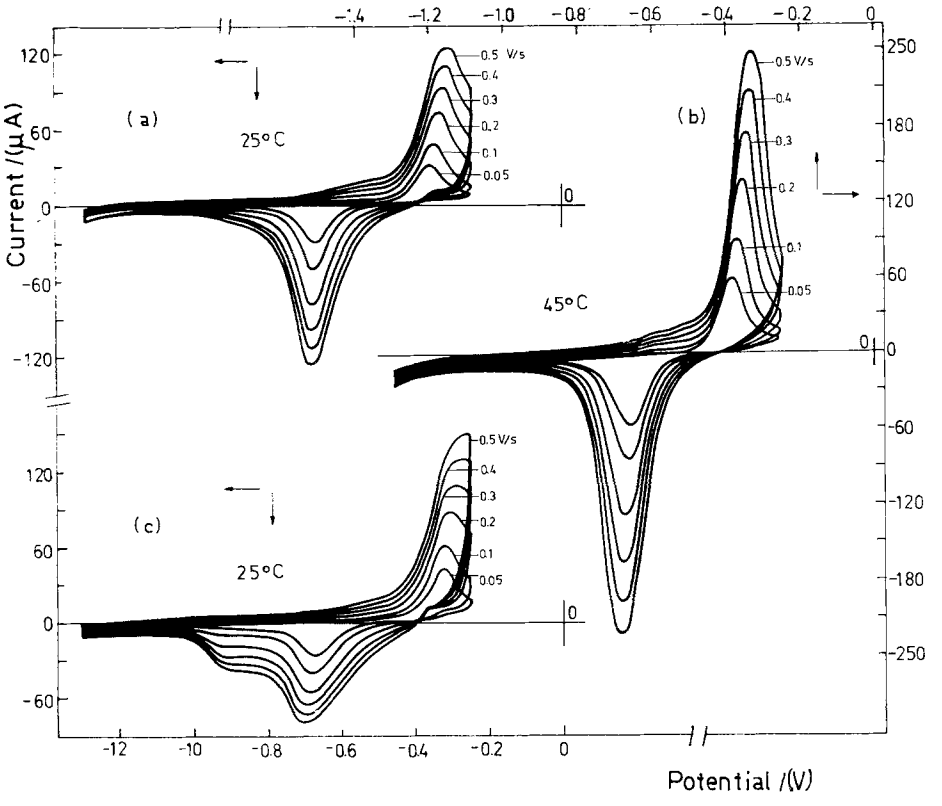

Fig. 10. Stabilized potentiodynamic E/I displays obtained with the same electrochemical interface at 25, 45 and 25° C. 0.1 M NaOH. Electrode area 0.0314 cm².

$0 \leqslant \tau \leqslant 30$ min (Fig. 13). Under these conditions, the potentiodynamic display involves a previously oxidized surface at a constant potential corresponding to the initiation of Cu_2O formation. The E/I display recorded immediately after the potential holding shows that the cathodic current peak is narrower than in the conventional triangular potential sweep E/I profile. The same result is obtained if after holding the potential at E_τ during the time τ, the circuit is open for 15 min before the E/I profile is recorded (Fig. 13c). These E/I displays, however, are unstable since they pro-

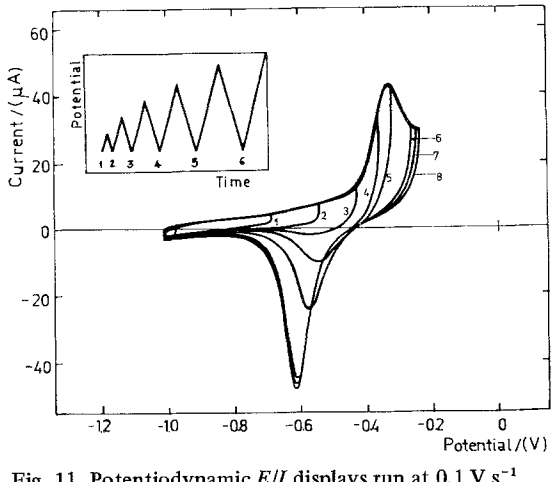

Fig. 11. Potentiodynamic E/I displays run at 0.1 V s^{-1} including a gradual change of $E_{\lambda,a}$ in the order indicated by the numbers. 0.1 M NaOH + 0.5 M $NaClO_4$, 25° C. Electrode area 0.0314 cm².

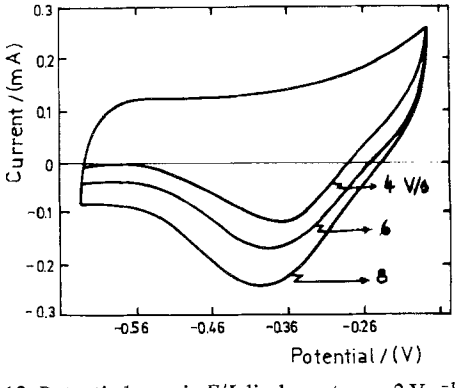

Fig. 12. Potentiodynamic E/I displays at $v_a = 2$ V s^{-1} and different v_c.

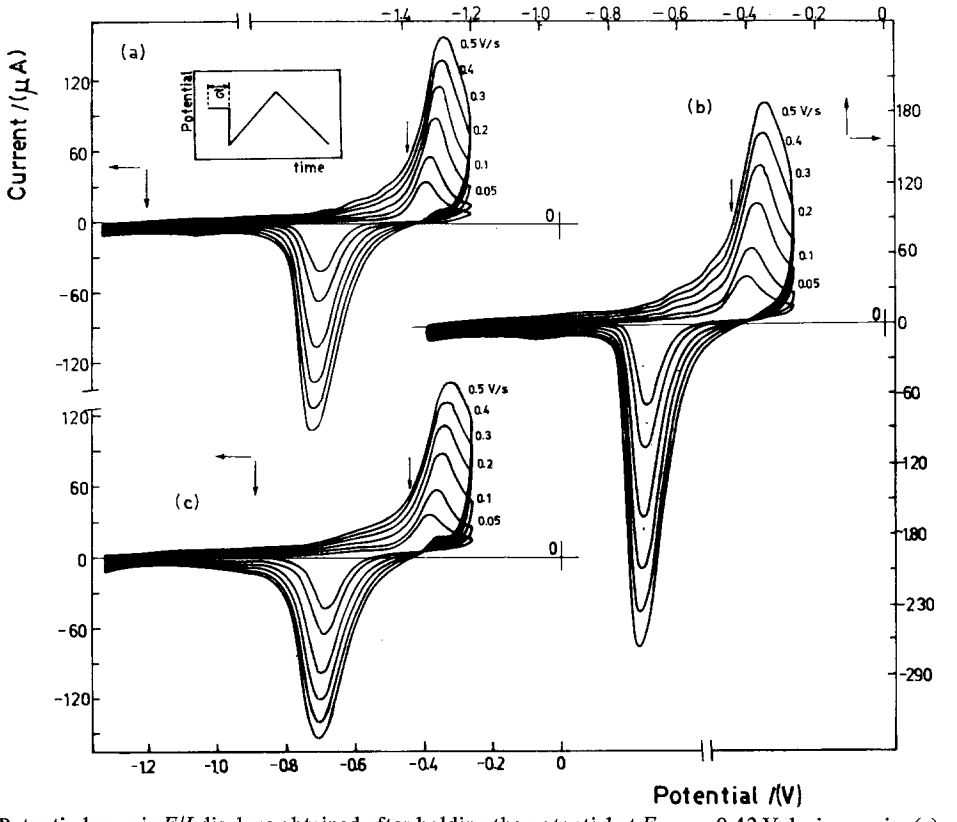

Fig. 13. Potentiodynamic E/I displays obtained after holding the potential at $E_\tau = -0.42$ V during τ min. (a) $\tau =$ 15 min; (b) $\tau = 30$ min; (c) $\tau = 30$ min followed by 15 min open circuit before the potential sweep. 0.1 M NaOH, 25° C. Electrode area 0.0314 cm^2.

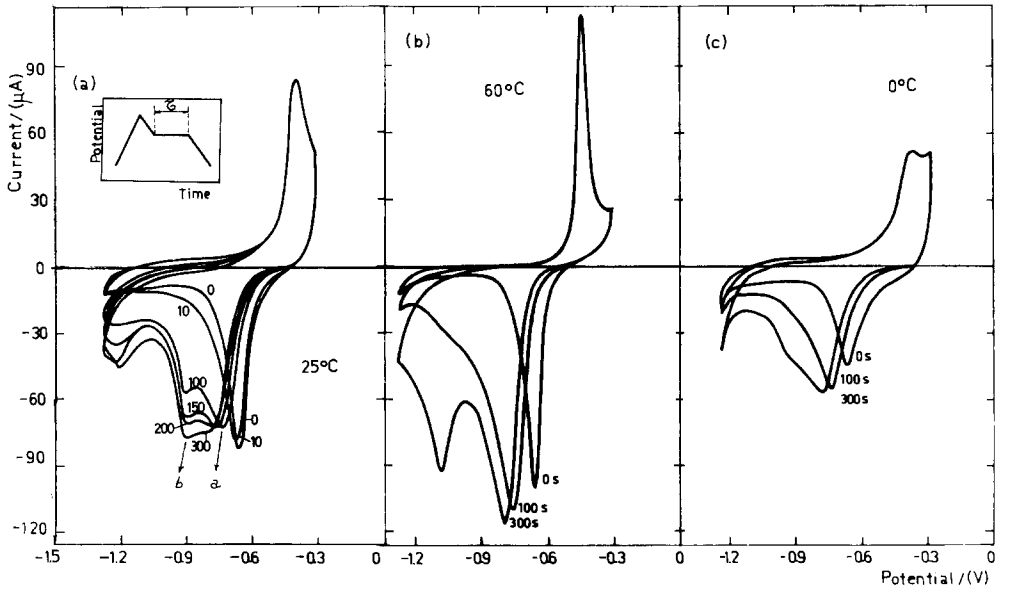

Fig. 14. Potentiodynamic E/I displays at 0.1 V s^{-1} including a potential holding during the negative-going potential excursion, at $(E_\tau)_{i\to 0}$, 1 M NaOH. (a) 25° C; (b) 60° C and (c) 0° C. Electrode area 0.0314 cm^2.

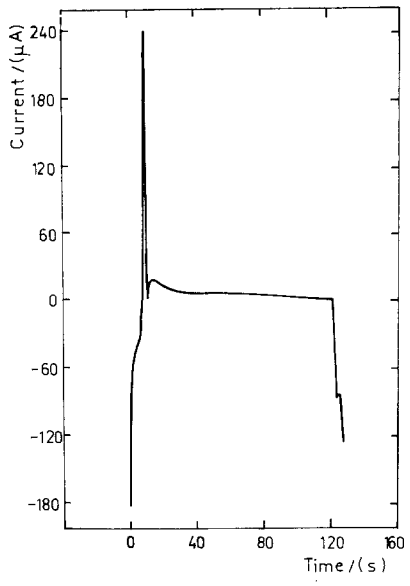

Fig. 15. Current transient recorded at $(E_\tau)_{i\to 0}$ under the experimental conditions described in Fig. 14.

gressively recover the characteristics already described in the absence of the potential holding simply through continuing the repetitive triangular potential sweeps.

The occurrence of the complex cathodic E/I contour is also confirmed by means of the following potential–time perturbation programme. The Cu_2O layer is firstly formed at v_a and during the reverse potential excursion, the potential is held for a certain pre-fixed lapse at a value $(E_\tau)_{i\to 0}$ where the net current approaches the smallest possible value (Fig. 14). The transient current at this potential is always anodic (Fig. 15).

At $(E_\tau)_{i\to 0}$ possible transformations of the anodic species occur either chemically or electrochemically as observed through a net separation of the anodic current peaks ascribed to the Cu(I) species. This effect is enhanced at 60° C (Fig. 14). Nevertheless, taking into account the $E_{\lambda,a}$ values reached during the potential scanning, throughout the anodic process the formation of minor quantities of Cu(II) species cannot be disregarded. However, the API results are sharper and more symmetric than those at lower temperatures. After holding the potential at $(E_\tau)_{i\to 0}$ an increase of the cathodic charge is observed as the holding time increases. The E/I profile continues towards negative potentials and then presents two current peaks (a and b) which are located at more negative potentials than that of CPI. The systematic shift of CPI with τ, the time the potential is held at $(E_\tau)_{i\to 0}$, suggests that the anodic current peak a contains a relatively large contribution of CPI which moves towards more negative potentials as τ increases. The current peak height ratio, I_a/I_b, decreases and the cathodic current at $E_{\lambda,c}$ becomes larger as τ increases. Moreover, in this case, a third cathodic current peak is recorded directly in the potential range where the hydrogen evolution takes place. This corresponds to an apparent depolarization effect of the hydrogen evolution reaction on copper in the alkaline solution.

4. Discussion

The complex negative-going potential E/I displays in the Cu/Cu_2O potential range indicate that the overall reduction of the Cu(I) species anodically formed is a composite process, although the current efficiency for the potentiodynamic electrochemical formation and dissolution of the Cu(I)-containing film is always about 100%. Therefore, the electrochemical reaction can be interpreted assuming that during the potentiodynamic perturbation, different species are formed both through the proper electrochemical reaction and because of the subsequent different transformations involving the species formed during the electrochemical reaction. Under potentiodynamic conditions the composition of the anodic film appears as dependent on the perturbation programme [14, 15].

To attempt an explanation of the possible reaction pathway involved in the Cu_2O formation, the following relevant facts are considered. (a) The anodic charge decreases as v increases and a finite charge value is obtained by extrapolation to $v\to\infty$. Under these circumstances the shape of the cathodic E/I profile as well as the thickness of the Cu_2O layer formed are strongly influenced by the time interval spent between the anodic and the cathodic processes and by the rate of the potentiodynamic perturbation although according to electron microscopy data the final predominant structure resulting within the potential range investigated is Cu_2O [10]. Then, for constants E_s values and electrolyte composition the Cu_2O charge extrapolated to infinite potential sweep rate corresponds to a layer thickness involving only a few Cu_2O unit cells. Thus, if one takes a value 0.37 mC cm^{-2} for the Cu_2O monolayer [5] and the roughness factor

is supposed to be equal to one, the average thickness of the Cu_2O layer should be approximately five times larger than that of the single monolayer but, if the roughness factor is taken as equal to five, then only a single monolayer should be produced. On the other hand, the density of the anodic film was estimated [13] as 4.8 g cm^{-3}, a value which is lower than 6.0 g cm^{-3}, the density of crystalline Cu_2O [5]. This difference can be interpreted either by assuming that the growth of the Cu_2O layer occurs in patches that gradually spread to form the loose structure Cu_2O film or by admitting that the film structure implies Cu_2O and CuOH species as simultaneous components of the anodic film [14, 15]. The former concept has been used to calculate the optical characteristics of Cu_2O film formation on the basis that the latter are not linear with film thickness [12]. The second alternative which is justified by the optical data [10] would mean that the ratio of the Cu_2O to CuOH species in the film should also be time dependent. Therefore, the properties derived from films produced under stationary conditions cannot be straightforwardly extended to films which are produced under potentiodynamic conditions.

(b) The complex dependence of the anodic and the main cathodic current peaks on v either obtained from the first or from the nth E/I displays should also be considered as a relevant factor. No simple I_p versus $v^{1/2}$ nor I_p versus v linear relationships are observed. This indicates that the electrochemical reaction is more complex than either a simple diffusional or a nucleation and growth mechanism. Probably the electrochemical reaction involves a contribution of both mechanisms.

The most reliable kinetic data associated with CPI, namely to the reduction of the Cu_2O species, is obtained at Q_a = const, (Fig. 16) when the negative-going potential scan is interrupted for a certain time at the potential where the current is null. Under these circumstances, the height of CPI increases linearly with v, and its potential changes linearly with log v, involving a slope slightly higher than 60 mV/decade at 25° C.

On the other hand, the kinetic data corresponding to the Cu_2O formation cannot be straightforwardly normalized as is the case for the reduction process. The Tafel plots obtained from the ascending portion of the potentiodynamic E/I profiles depend noticeably on the perturbation conditions and the corresponding slopes vary between 50 and 100 mV/decade, at 25° C, for 2 M NaOH solution (Fig. 17). However, as this corresponds to an interface whose average composition and energetics are

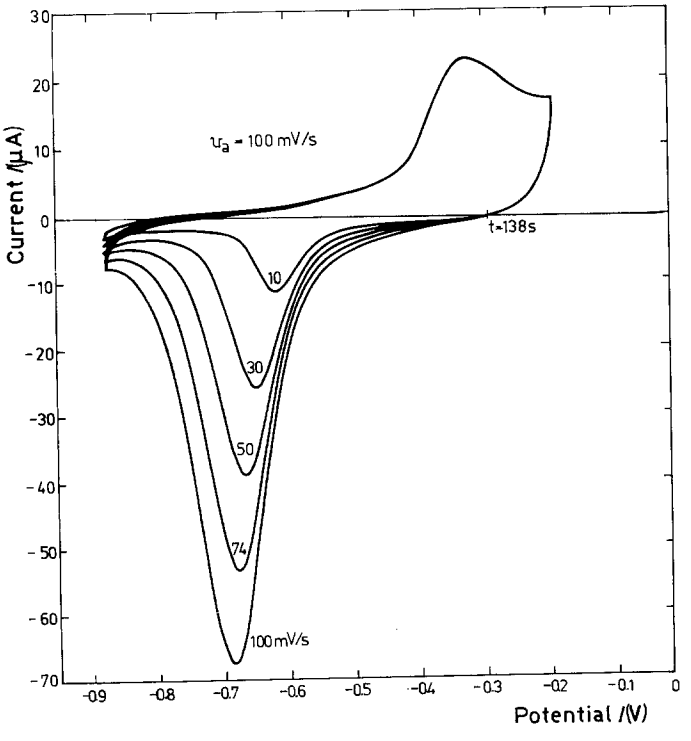

Fig. 16. Potentiodynamic E/I displays at $v_a = 0.1$ V s^{-1} and different v_c including an interruption of the potential sweep at − 0.3 V for 138 s. 0.01 M NaOH + 0.3 M $NaClO_4$, 25° C. Electrode area 0.0314 cm^2.

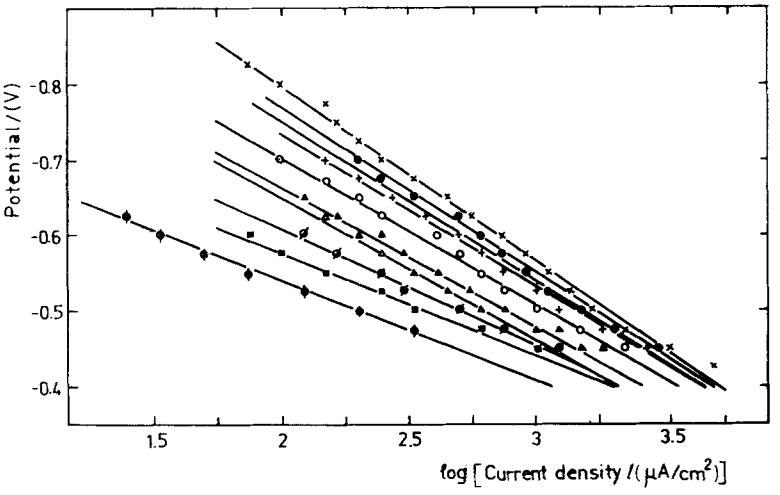

Fig. 17. Tafel plots derived from the ascending portion of the API profile at different potential sweep rates. 2 M NaOH, 25° C.

time dependent, the Tafel slope is, in principle, mechanistically irrelevant.

(c) It is also interesting to note that while only a single anodic current peak is recorded under any circumstances, a multiplicity of cathodic current peaks are observed. The total charge in the overall cathodic reaction seems to be independent of the distribution of the cathodic current peaks. This confirms that different species which are picked up during the reduction process are formed during the anodic reaction. Therefore, the anodic reaction itself should be considered as a complex process which generates different species through electron transfer processes coupled with chemical side reactions.

The results obtained at high v and those with increasing $E_{\lambda,\,a}$ within the potential range preceding that of API, suggest that one of the species initially formed participates in a fast reduction process. If the initial species is not rapidly reduced it undergoes a chemical change yielding the more stable components of the Cu(I)-containing film. These electrochemical characteristics can be ascribed to the initial formation of soluble Cu(I) species in the course of the anodic reaction. This conclusion has already been derived from the chronopotentiometric transition time related to Cu_2O formation [11] and through earlier results obtained with a rotating disc and split ring electrode [4]. Therefore, the initial stage in the electro-oxidation process can be given according to one of the following electrochemical dissolution reactions:

$$Cu + 2\,OH^- \rightleftharpoons Cu(OH)_2^- + e \qquad (1a)$$

$$Cu + 2\,H_2O \rightleftharpoons Cu(OH)_2^- + 2\,H^+ + e \qquad (1b)$$

According to equilibrium data the soluble Cu(I) aqueous ion is unstable and decomposes thus yielding the insoluble Cu_2O species [20] according either to

$$2\,Cu(OH)_2^- + 2\,H^+ \rightleftharpoons Cu_2O + 3\,H_2O \qquad (2)$$

or to

$$2\,Cu(OH)_2^- \rightleftharpoons Cu_2O + H_2O + 2\,OH^- \qquad (3)$$

The fast response of the negative-going potential E/I profile involving $E_{\lambda,\,a}$ values smaller than the potential of the anodic current peak related to the Cu_2O formation can be interpreted as the reduction of the Cu(I) soluble species according to Reaction 1. The charge of the latter picked up during the reduction process increases when the time elapsed between the positive-going and the negative-going potential excursions decreases. This implies that in the course of the reaction the soluble Cu(I) species is electrochemically more reactive than any Cu_2O species resulting from Reaction 2 [14, 15]. Therefore, Reactions 1 and 2 correspond to the electrochemical dissolution–chemical precipitation mechanism of Cu_2O film growth [7, 9, 11, 13]. However, a straight-forward

distinction between the possible reaction mechanisms using only the data obtained from non-stationary perturbation techniques involving different time scales seems rather difficult since in dealing with film forming processes the contribution of the different stages of the reaction as well as the composition of the film formed [10] may change with the perturbation conditions applied to the electrochemical interface.

The multiplicity of peaks related to the cathodic processes coincides in number with that recently reported for the Cu/0.1 M LiOH interface [15]. Besides the reduction current related to the soluble Cu(I) species, there are at least another two contributions involving Cu_2O species of appreciably different reactivities, as deduced from the remaining cathodic current peaks. There is evidence that one of these species whose reduction peak potential is more negative disappears when the potentiodynamic sweep is preceded by a potential holding at values prior to the API potential (Fig. 13). Since the cathodic charge in those experiments remains constant it suggests that one of the species has been transformed into the other involving the reduction current peak at more positive potentials. An interpretation of these reactions can be advanced in terms of the reaction pathway previously postulated for the potentiodynamic behaviour of Cu in alkaline solutions involving the formation of intermediate OH-containing surface species [14]. Accordingly the species which is reduced at more negative potentials can be related to those containing the most strongly bound OH entities. The possible cathodic step can be put forward as follows:

$$Cu(OH) + e \rightleftharpoons Cu + OH^-. \qquad (4)$$

Therefore, the disappearance of the cathodic current peak located at more negative potentials can be interpreted as a decreasing contribution of the CuOH species in the reduction process. Processes such as Reaction 4 are usually found during the passivation of metals in aqueous electrolytes [21, 22]. Therefore, the Cu(OH), $Cu(OH)_2^-$, and Cu_2O can be considered as the main reactants associated respectively to Reactions 4 and to Reactions 1–3 in the reverse direction which are revealed through the E/I display run in the negative-going potential excursion. The three species, however, are probably linked through chemical reactions such as:

$$2\,Cu(OH) \rightleftharpoons Cu_2O + H_2O \qquad (5)$$

which occur in parallel with the electrochemical processes.

The present results, therefore, show that Cu_2O film formation involves the occurrence of non-equilibrium states, similar to those already described for other anodic oxygen-containing layers, either mono- or multilayer, in different electrolytes [23–25]. The ageing at a constant potential in the potential range of API implies an anodic transient current (Fig. 15) which is associated with the charge increase of the passivating layer. But in this case, the multiplicity and shift of cathodic current peaks can be well distinguished (Fig. 14). This, at least in part, explains the failure to interpret the Cu_2O electrochemical processes exclusively in terms of a single reaction mechanism involving either a nucleation and growth process, or a simple precipitation and chemical dissolution mechanism. Nevertheless, it should be recognized that the dependence of the film thickness on v, and consequently the film thickness changing inversely with v, may result from any reaction model where the rate of accommodation of the species for the growing process lags the potential perturbation rate.

Despite the composite structure of the Cu_2O anodic film, the kinetic law corresponding to the film thickening can be derived from runs such as that shown in Fig. 15. Thus, after holding the potential during the pre-set time in the potential range where Cu_2O is formed, the thickness of the anodic layer can be determined through the corres-

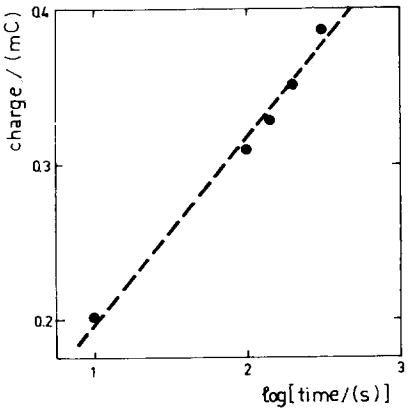

Fig. 18. Plot of the cathodic charge versus τ. Data obtained from the runs shown in Fig. 14a.

ponding reduction charge. Taking into account that within the potential range of Cu_2O formation the Q_a/Q_c ratio is practically one, the relative anodic charge measured through the charge involved in the negative-going potential excursion increases linearly with the logarithm of the potentiostating time (Fig. 18) for any of the experimental conditions covered in the present work. Under comparable conditions the charge increase is more noticeable as the temperature increases. The greatest charge increase observed at the highest temperature is probably due, despite the larger overall depolarization of the electrochemical reaction, to an increasing roughness of the electrode.

Acknowledgement

INIFTA is sponsored by the Consejo Nacional de Investigaciones Científicas y Técnicas, the Universidad Nacional de La Plata and the Comisión de Investigaciones Científicas (Pcia. de Bs.As.). This work is also partially supported by the Regional Program for the Scientific and Technological Development of the Organization of the American States.

References

[1] U. Bertocci and D. R. Turner in 'The Encyclopedia of the Electrochemistry of the Elements' (Edited by A. J. Bard) Vol. II, M. Dekker, New York (1974) ch. 6, p. 384.
[2] E. Mueller, *Z. Elektrochem.* **13** (1907) 133.
[3] J. S. Halliday, *Trans. Faraday Soc.* **50** (1954) 171.
[4] B. Miller, *J. Electrochem. Soc.* **116** (1969) 1675.
[5] N. A. Hampson, J. B. Lees and K. I. MacDonald, *J. Electroanalyt. Chem.* **32** (1971) 165.
[6] M. J. Dignam and D. B. Gibbs, *Canad. J. Chem.* **48** (1970) 1242.
[7] J. Ambrose, R. G. Barradas and D. W. Shoesmith, *J. Electroanalyt. Chem.* **47** (1973) 47.
[8] *Idem, ibid* **47** (1973) 65.
[9] T. Yoshimura, Y. Imanaka and M. Yamashita, *Sci. Eng. Rev. Doshisha Univ.* **14** (1974) 247.
[10] D. W. Shoesmith, T. E. Rummery, D. Owen and W. Lee, *J. Electrochem. Soc.* **123** (1976) 790.
[11] V. Ashworth and D. Fairhurst, *ibid* **124** (1977) 506.
[12] A. G. Akimov, M. G. Astafiev and I. R. Rozenfeld, *Elektrokhim.* **13** (1977) 1493.
[13] M. Yamashita, *Seventh International Congress on Metal. Corr.*, Rio de Janeiro (1978).
[14] A. M. Castro Luna de Medina, S. L. Marchiano and A. J. Arvia, *J. Appl. Electrochem.* 8 (1978) 121).
[15] S. Fletcher, R. G. Barradas and J. D. Porter, *J. Electrochem. Soc.* **125** (1978) 1960.
[16] S. N. Raicheva and D. J. Zlateva, *C. R. Acad. Bulg. Sci.* **27** (1947) 1695.
[17] *Idem, ibid* **28** (1975) 955.
[18] *Idem, ibid* **30** (1977) 1443.
[19] *Idem, ibid* **30** (1977) 1573.
[20] A. M. Castro Luna, S. L. Marchiano and A. J. Arvia, *J. Electronanalyt. Chem.* **59** (1975) 335.
[21] M. Pourbaix, 'Atlas of Electrochemical Equilibrium in Aqueous Solutions', Pergamon Press, Oxford (1966).
[22] V. Brusic and T. J. Watson, 'Oxides and Oxide Films' (Edited by J. W. Diggle) Vol. 1, M. Dekker, New York (1972) ch. 1.
[23] A. J. Arvia, *Isreal J. Chem.*, (in press).
[24] R. Cordova O., M. E. Martins and A. J. Arvia, *J. Electrochem. Soc.* **126** (1979) 172.
[25] R. Schrebler G., J. R. Vilche and A. J. Arvia, *J. Appl. Electrochem.* **9** (1979) 183.